Acta Crystallographica Section A
Foundations of Crystallography
ISSN 0108-7673

Received 25 December 2006
Accepted 10 April 2007

Scaling behaviour of pair correlation functions for randomly faulted hexagonal close-packed structures

Pratyush Tiwary[a] and Dhananjai Pandey[b]*

[a]Department of Metallurgical Engineering, Banaras Hindu University, Varanasi 221005, India, and [b]School of Materials Science and Technology, Banaras Hindu University, Varanasi 221005, India. Correspondence e-mail: dpandey@bhu.ac.in

Monte Carlo simulations and analytical results are used to demonstrate that the hexagonal close-packed (h.c.p.) pair correlation functions for different values of randomly distributed growth and deformation faults can be collapsed into master curves when plotted against a spatial variable, scaled with respect to a characteristic length (L). The functional dependences of L on different types of faults are found to be non-universal. A simple method for the determination of L from the measured intensity distributions is also outlined.

1. Introduction

Stacking faults are commonly observed in several types of layered materials such as SiC, ZnS, CdI_2, micas, Co and its alloys, close-packed martensite phases of copper-based alloys and alkali metals, hexagonal C_{70} *etc.* (Pandey & Krishna, 1982; Berliner *et al.*, 1989, 1992; Blanc *et al.*, 1996). Stacking faults introduced during plastic deformation of metals are commonly called deformation faults which result from the shearing of one part of a crystal past another across close-packed planes (Warren, 1969). The faults which result from accidental mistakes during crystal growth are termed growth faults (Pandey & Krishna, 1982). During irradiation of metals and alloys, extrinsic faults involving precipitation of vacancies are commonly observed (Hirth & Lothe, 1968). All these types of faults are usually distributed randomly. However, when faults are introduced during phase transformations between two close-packed or layered structures, the distribution no longer remains random but instead becomes non-random as was first noted in the context of 2*H* to 6*H* transformation in SiC involving layer displacement faults (Pandey *et al.*, 1980*a*,*b*,*c*).

The first systematic treatment of diffraction from faulted close-packed structures was given by Wilson (1942) and Hendricks & Teller (1942). Since then, several workers have developed theories of diffraction from various close-packed structures containing different geometrical types of randomly as well as non-randomly distributed stacking faults (Wilson, 1962; Warren, 1969; Pandey & Krishna, 1992). Use of Monte Carlo techniques leads to the same results as those obtained by analytical treatment for random distribution of stacking faults (Berliner & Werner, 1986). However, for non-random distribution of faults, the Monte Carlo results have been shown to be different from those obtained analytically using the difference equation approach especially for large fault probabilities α (Kabra & Pandey, 1995, 1996; Shreshtha *et al.*, 1996). The main difference between the analytical and Monte Carlo approaches is that the latter leads to the arrest of the transformation for an intermediate value of non-random fault probability α less than the value of unity required for completion of the transformation. Kabra & Pandey (1988) and subsequently Shreshtha & Pandey (1996, 1997) have also used one-dimensional kinetic Ising models based on Glauber and Kawasaki dynamics to study the 2*H* to 6*H* and 2*H* to 3*C* transformations. These models predict arrest of transformation for the Kawasaki dynamics (which represents insertion of layer displacement faults) only and not for Glauber dynamics (which corresponds to the insertion of deformation faults). In the Monte Carlo approach, Fourier transform of the ensemble averaged pair correlation functions, calculated numerically using simulated sequences of close-packed layers generated by a specific algorithm, directly gives the intensity distribution for faulted structures. The Monte Carlo technique is fairly general and can handle mixtures of stacking faults of all types in all concentrations, in contrast to the analytical techniques which are usually intractable for large fault probabilities and also for mixed faulting.

In addition to the fault model approach, it is also possible to describe a faulted crystal without specifying the nature and geometry of stacking faults explicitly and carry out the calculation of diffracted intensity in the manner described by various workers (Zachariasen, 1947; Farkas-Jahnke, 1973; Estevez-Rams *et al.*, 2001; Varn *et al.*, 2002). By Fourier inversion of the observed intensity distribution along diffuse streaks, one can obtain the relevant pair correlation functions which carry information about the different types of stacking faults present in a particular crystal (Estevez-Rams *et al.*, 2001; Estevez-Rams, Leoni *et al.*, 2003; Estevez-Rams, Aragon-Fernandez *et al.*, 2003). However, the task of extracting the faulted stacking sequence from the pair correlation functions is formidable, unless the stacking-fault model is known. Thus the practical utility of the so called 'direct' methods, advanced in recent years, is somewhat limited. This limitation is similar to the problem of determining the correct crystal structure

from the Patterson function (which is the same as the pair correlation) for ordered structures (Warren, 1969). Attempts to fit the observed intensity distributions, such as those recently given by Varn *et al.* (2002), without taking care of convolution effects (Pandey *et al.*, 1986) and beam-divergence effects (Pandey *et al.*, 1987) present in the experimental profiles have little meaning in a quantitative sense.

In the Monte Carlo simulation for non-random faulting using kinetic Ising models, Shreshtha & Pandey (1996, 1997) and Shreshtha *et al.* (1996) demonstrated that the pair correlation functions $P(m)$, $Q(m)$ and $R(m)$ can be described by exponentially varying functions like $\exp(-m/L)$, where L is a characteristic length scale. This type of exponentially varying function has subsequently been used by Estevez-Rams, Leoni *et al.* (2003) in the context of random growth and deformation faults in face-centred cubic (f.c.c.) crystals. Shreshtha & Pandey (1996, 1997) have also demonstrated the scaling behaviour of the pair correlation functions in the time domain for Glauber dynamics (non-random deformation faults). In the present work, we have performed Monte Carlo simulations for random distributions of growth and deformation faults as well as their mixtures in h.c.p. crystals to demonstrate that the scaling behaviour holds true in the fault probability domain also. We also show that the characteristic length scale L used in scaling can be described by polynomials of second or higher order in fault probabilities. The dependence of the characteristic length scale on fault probabilities as obtained by simulations is shown to be in good agreement with those derived analytically. The exact relationship between the characteristic length scale and the full width at half-maximum of the diffuse peaks is also presented.

2. Basic diffraction equations for h.c.p. crystal with random growth and deformation faults

Consider a stack of N close-packed layers numbered as $j = 0$ to $N - 1$. The resulted diffracted intensity, I, from such a stack of layers can be written as (Shreshtha & Pandey, 1996)

$$I = (1/N) + 2\sum_{m=1}^{\infty}\frac{N-m}{N^2}\big(\{P(m) + [Q(m) + R(m)]\cos(\theta)\}\cos(m\varphi) + [Q(m) - R(m)]\sin(\theta)\sin(m\varphi)\big), \quad (1)$$

where $\phi = \pi h_3$, h_3 being a continuous variable along $\mathbf{c}^*$, $\theta = 2\pi(H - K)/3$, and $P(m)$, $Q(m)$ and $R(m)$ are the pair correlation functions defined as the probabilities of finding A–A, B–B, C–C; A–B, B–C, C–A; and A–C, B–A, C–B type pairs of layers with m layer separations, such that

$$P(m) + Q(m) + R(m) = 1 \quad (2)$$

and

$$Q(m) = R(m). \quad (3)$$

Using the earlier formulation of Pandey & Krishna (1977), $P(m)$ for h.c.p. crystal containing random growth and deformation faults can be written as

$$P(m) = 2/3[1/2 + c_0\rho_0^m + c_e\rho_e^m], \quad (4)$$

where the constants c_e, c_o, ρ_e and ρ_o are functions of the growth (α) and deformation (β) fault probabilities as given below:

$$\rho_e = 1/2(\alpha - x), \quad (5)$$

$$\rho_o = -1/2(\alpha + x), \quad (6)$$

$$c_e = 1/2[1 - (1 - \alpha)/x] \quad (7)$$

and

$$c_o = 1/2[1 + (1 - \alpha)/x], \quad (8)$$

where

$$x = \big(\{\alpha - 4(1-\gamma) - 2[(3-4\gamma)(1-\gamma)]^{1/2}\} \times \{\alpha - 4(1-\gamma) + [(3-4\gamma)(1-\gamma)]^{1/2}\}\big)^{1/2} \quad (9)$$

and

$$\gamma = 3\beta(1 - \beta). \quad (10)$$

The quantities c_e, c_o, ρ_e and ρ_o will be real or imaginary depending on the value of x. Two cases arise:

case 1: $0 < \alpha < 4(1-\gamma) - 2[(3-4\gamma)(1-\gamma)]^{1/2}$

case 2: $4(1-\gamma) - 2[(3-4\gamma)(1-\gamma)]^{1/2} < \alpha < 1.$

For case 1, $\{\alpha - 4(1-\gamma) + 2[(3-4\gamma)(1-\gamma)]^{1/2}\}$ is negative and hence x will be a real quantity. For case 2, $\{\alpha - 4(1-\gamma) + 2[(3-4\gamma)(1-\gamma)]^{1/2}\}$ is positive so that x becomes an imaginary quantity. Thus, for case 1, c_e, c_o, ρ_e and ρ_o are real quantities, while, for case 2, c_e, c_o, ρ_e and ρ_o are all complex quantities. It can be shown easily that, for case 1, the average structure remains h.c.p.-like, whereas, for case 2, it becomes f.c.c.-like. These two cases are elucidated through regions A and B in Fig. 1, which is a plot of $4(1-\gamma) + 2[(3-4\gamma)(1-\gamma)]^{1/2}$ *versus* β. Case 1 will be applicable for combinations of fault probabilities α and β such that the relevant region in Fig. 1 is A; likewise for case 2. We shall now examine the scaling properties of the pair correlation function $P(m)$ for pure growth faulting, pure deformation faulting and mixed faulting separately.

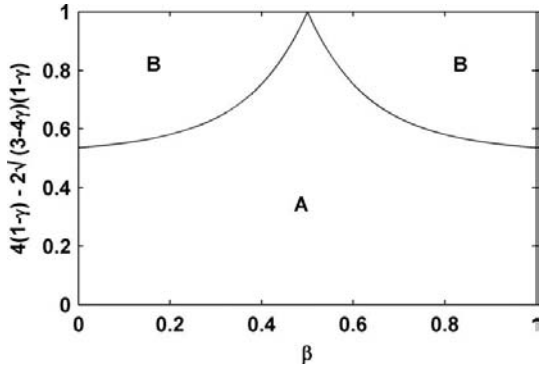

Figure 1
Demarcation of h.c.p.-like regions (A) and f.c.c.-like regions (B).

3. Scaling behaviour of pair correlation functions for faulted h.c.p. crystals

For Monte Carlo simulations, we start with an ensemble of layers arranged in the perfect h.c.p. manner (*i.e.* $ABABAB\ldots$) and numbered 1 to 10000. Faults were introduced in this stack of layers using a pseudo-random-number generator in the interval [1, 10000]. Various layers in this stack were selected for faulting using the integer pseudo-random numbers. After the desired number of layers had been faulted, the pair correlation functions, $P(m)$, $Q(m)$ and $R(m)$, were computed for this ensemble. It was found that averaging over 60 such ensembles smooths out any statistical fluctuations in the variation of the correlation functions with the spatial coordinate m.

3.1. Random deformation faults

For the insertion of deformation faults in the Monte Carlo scheme, the layers succeeding each randomly selected layer were shifted in cyclic ($A \rightarrow B$, $B \rightarrow C$, $C \rightarrow A$) or anti-cyclic ($A \rightarrow C$, $B \rightarrow A$, $C \rightarrow B$) manner, taking into account the consideration that no two successive layers should be alike. Every such site was blocked for further faulting. The number of faults to be inserted was decided by the deformation fault probability β ($0 < \beta < 1$). The variation of $P(m)$ with m for various values of deformation fault probabilities β is shown in Figs. 2(*a*) and 2(*b*). It is evident from this figure that $P(m)$ for m even decreases exponentially with increasing m, while it increases exponentially for m odd. The following exponential functions describe the dependence of $P(m)$ on m (Shreshtha & Pandey, 1996):

$$P(m) = 1/3 + (2/3)\exp(-m/L), \quad \text{for } m \text{ even}, \tag{11}$$

and

$$P(m) = 1/3 - (1/3)\exp(-m/L), \quad \text{for } m \text{ odd}. \tag{12}$$

Here, L is a characteristic length scale which may be determined by least-squares fitting of equations (11) or (12) to the numerical values of $P(m)$. The variation of the characteristic length scale L so obtained with β is shown in Fig. 3(*a*). The shortest correlation length for random deformation faults occurs at $\beta = 0.5$. For $\beta > 0.5$, the correlation length again starts increasing and, at $\beta = 1$, the $ABABAB\ldots$ stacking sequence becomes $ACACAC\ldots$, which is equivalent to the initial sequence with a shift of origin. The decay and growth of correlation length for $\beta < 0.5$ and $\beta > 0.5$ are demonstrated in Fig. 3(*a*).

Following Shreshtha & Pandey (1996), we define correlation length ξ as the value of m beyond which $P(m) \simeq 1/3$. The physical significance of this is that the probability of finding A-, B- or C-type layers at a separation of m layers becomes equal (*i.e.* $\sim$1/3) for $m \geq \xi$. This in turn implies that, for $m > \xi$, there is no correlation between the pairs of close-packed layers. It may be mentioned that this property of convergence

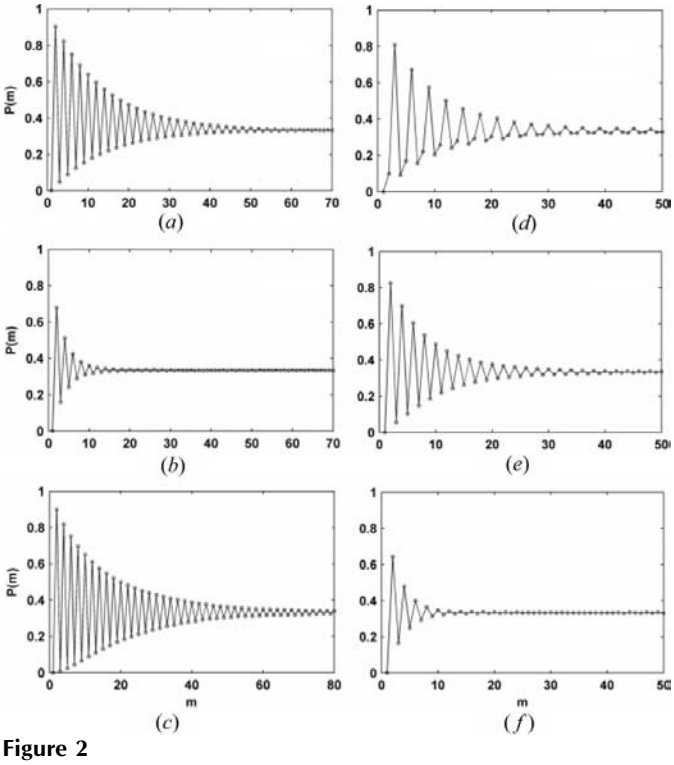

Figure 2
Variation of the pair correlation function $P(m)$ with the layer separation (m), for different values of the deformation fault probability β: (*a*) 0.05 and (*b*) 0.2; for different values of the growth fault probability α: (*c*) 0.1 and (*d*) 0.9; for mixed faulting with a fixed growth fault probability $\alpha = 0.1$ and variable deformation fault probability β: (*e*) 0.05 and (*f*) 0.2.

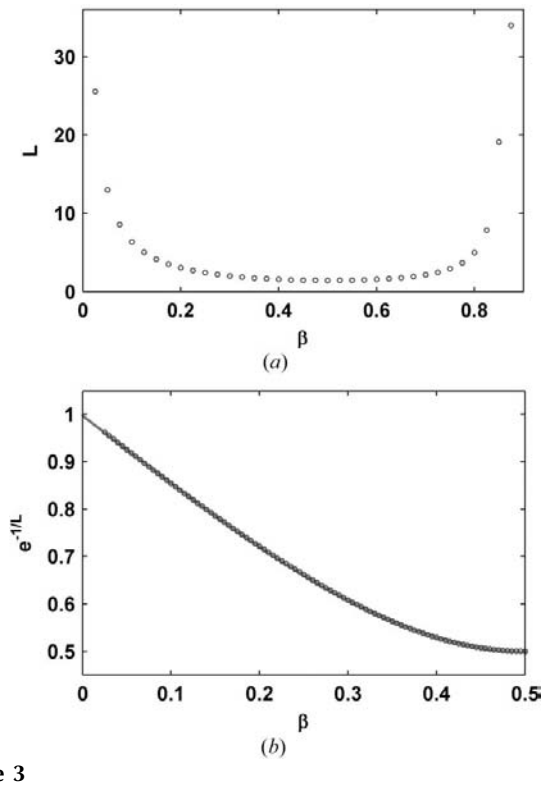

Figure 3
Variation of (*a*) the characteristic length scale (L) and (*b*) $\exp(-1/L)$ with the deformation fault probability β. Analytical results are denoted by empty circles while simulation results are denoted by the continuous curve.

of $P(m)$ to 1/3 is not universal; the exception being layer displacement faults in h.c.p. crystals which always retain long-range correlations (Sato, 1969; Pandey *et al.*, 1980*a*; Kabra & Pandey, 1995). The characteristic length scale (L) given by equations (11) and (12) is slightly less than the correlation length ξ as it corresponds to the value of m for which $\exp(-m/L)$ becomes $1/e$. However, it bears one-to-one correspondence with ξ, and is mathematically determinable unambiguously.

Instead of plotting $P(m)$ against m for various values of β as shown in Fig. 2, if we now plot $P(m)$ against a scaled variable m/L, all possible variations of $P(m)$ with m for various values of the fault probability, $0 < \beta < 0.5$, collapse into two master curves, one corresponding to the decay part and the other corresponding to the growth part. This is shown in Fig. 4 for $\beta = 0.1$, 0.2, 0.3 and 0.4 for the decay part only. Such a collapse of pair correlation functions into a master curve confirms the scaling property of $P(m)$ [as also of $Q(m)$ and $R(m)$] for random deformation faults.

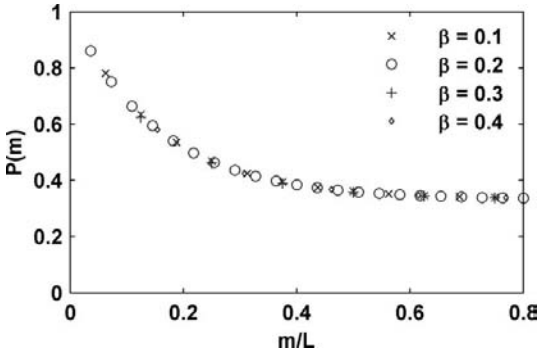

Figure 4
Variation of the decay part of $P(m)$ with scaled variable m/L for different deformation fault probabilities β, denoted by different symbols, exhibiting collapse of the entire data on a single master curve.

3.2. Random growth faults

For the insertion of growth faults, the orientations of each randomly selected layer and the subsequent alternate layers were changed cyclically or anti-cyclically keeping in mind the constraint that no two successive layers can be in the same orientation. The chosen site was blocked for further faulting. As is evident from Fig. 1, it is necessary to consider the results of simulation for the two ranges of $\alpha < 0.536$ and $\alpha > 0.536$ separately.

The variation of $P(m)$ with m for various values of growth fault probabilities (α) is shown in Figs. 2(*c*) and 2(*d*). The characteristic length scales (L) for different growth probabilities in the range $0 < \alpha < 0.536$ were obtained by least-squares fitting using equation (11). The variation of L with α is shown in Fig. 5(*a*). For the range $0.536 < \alpha < 1$, f.c.c. correlations start emerging, as can be seen from Fig. 2(*d*), and the functional forms given by equations (11) and (12) need to be modified as under

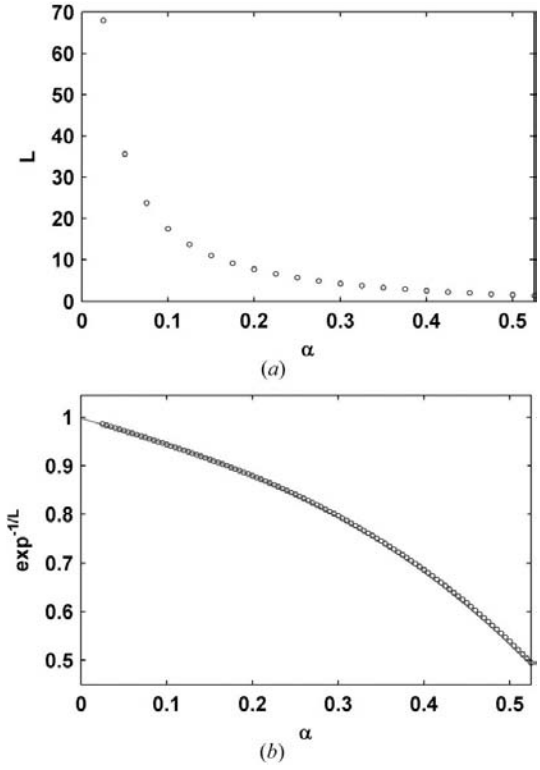

Figure 5
Variation of (*a*) the characteristic length scale (L), and (*b*) $\exp(-1/L)$ with the growth fault probability α for the range $0 < \alpha < 0.536$. Analytical results are denoted by empty circles while simulation results are denoted by the continuous curve.

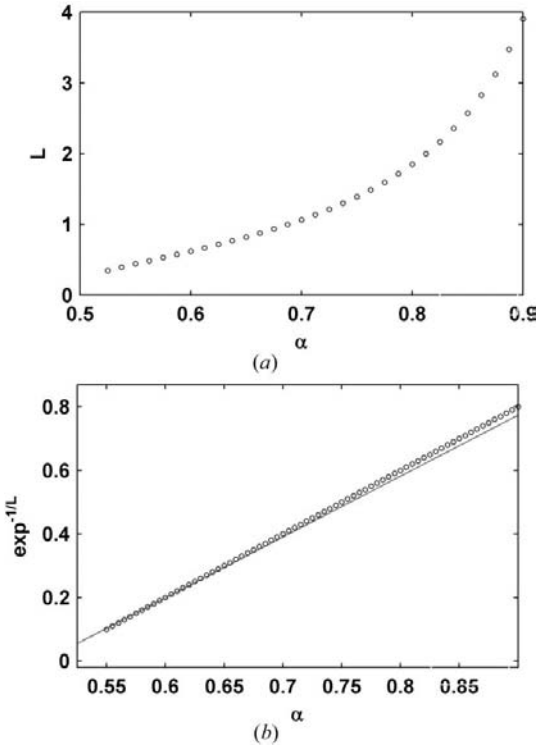

Figure 6
Variation of (*a*) the characteristic length scale (L) and (*b*) $\exp(-1/L)$ with the growth fault probability α for the range $0.536 < \alpha < 1$. Analytical results are denoted by empty circles while simulation results are denoted by the continuous curve.

$$P(m) = 1/3 + (2/3)\exp(-m/L), \quad \text{for } m = 0 \bmod 3, \quad (13)$$

and

$$P(m) = 1/3 - (1/3)\exp(-m/L), \quad \text{for } m = 1, 2 \bmod 3. \quad (14)$$

The variation of the characteristic length scale L with α for this range of values is shown in Fig. 6(*a*).

It is found that for both ranges of values of α, *i.e.* $0 \leq \alpha < 0.536$ and $0.536 < \alpha \leq 1$, the values of $P(m)$ can be collapsed into master curves on plotting $P(m)$ against m/L, as shown in Figs. 7(*a*) and 7(*b*) for the decay part of $P(m)$ for the two ranges of values of α. These collapses confirm the scaling property of the pair correlation functions for h.c.p. crystals with random growth faults for all values of the fault probability.

3.3. Mixed random growth and random deformation faults

We now consider a mixture of growth and deformation faults. For simulations, we have fixed the growth fault probability at $\alpha = 0.1$ and vary β in the range 0 to 1.

For mixed faulting, we first introduce growth faults in a stack of 10000 layers, as per the Monte Carlo scheme outlined in §3.2. Deformation faults were introduced in this growth faulted stack of layers. The variation of $P(m)$ with m for $\alpha = 0.1$ and $0 < \beta < 1$ is shown in Figs. 2(*e*) and 2(*f*). Fig. 8(*a*) shows the variation of the characteristic length scale L with β. For $\beta < 0.4$, the h.c.p. characteristic length scale decreases with increasing β but the trend is reversed for $\beta > 0.4$. This case is to be contrasted with that of pure deformation faulting where the reversal of the trend of the L *versus* β plot occurred at $\beta \approx 0.5$.

When we plot $P(m)$ against the scaled variable m/L, the values of $P(m)$ collapse into two master curves corresponding to the decay and growth parts of $P(m)$ for the range of deformation fault probability, $0 \leq \beta < 0.4$. This is shown in Fig. 9 for the decay part. Similar collapses occur for $\beta > 0.4$. This confirms the scaling behaviour of pair correlation functions for mixed random faulting also.

4. Comparison of simulation results with analytical results

In this section, we shall consider the determination of the characteristic length scales for the three cases considered in the previous sections using the analytical treatment given in §2. Using equations (4)–(10), the general analytical expression for $P(m)$ can be written as

$$P(m) = 1/3\left\{1 + \left[1 + \frac{1-\alpha}{x}\right]\cos(m\pi)\left(\frac{\alpha + x}{2}\right)^m + \left[1 - \frac{1-\alpha}{x}\right]\cos(m\pi)\left(\frac{\alpha - x}{2}\right)^m\right\}. \quad (15)$$

On comparing the above equation with equation (11), we obtain

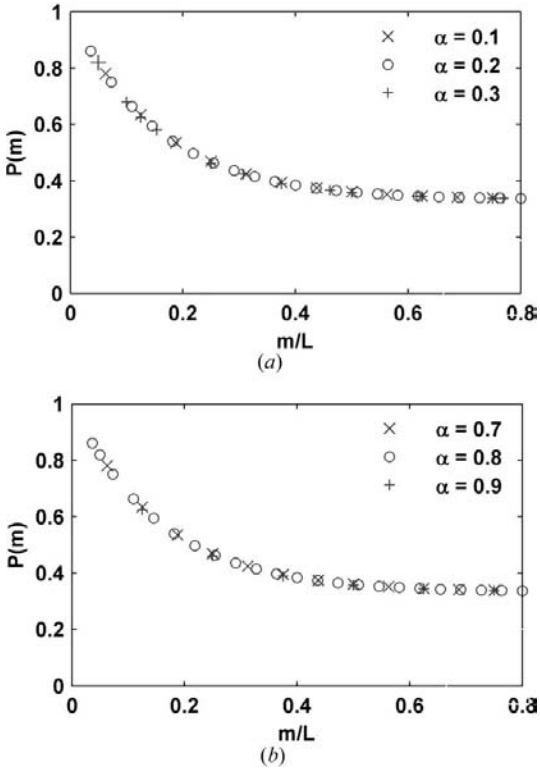

Figure 7
Variation of decay part of $P(m)$ with scaled variable m/L for different growth fault probabilities α, denoted by different symbols, exhibiting collapse of the entire data on a single master curve for case (*a*) $0 < \alpha < 0.536$ and (*b*) $0.536 < \alpha < 1$.

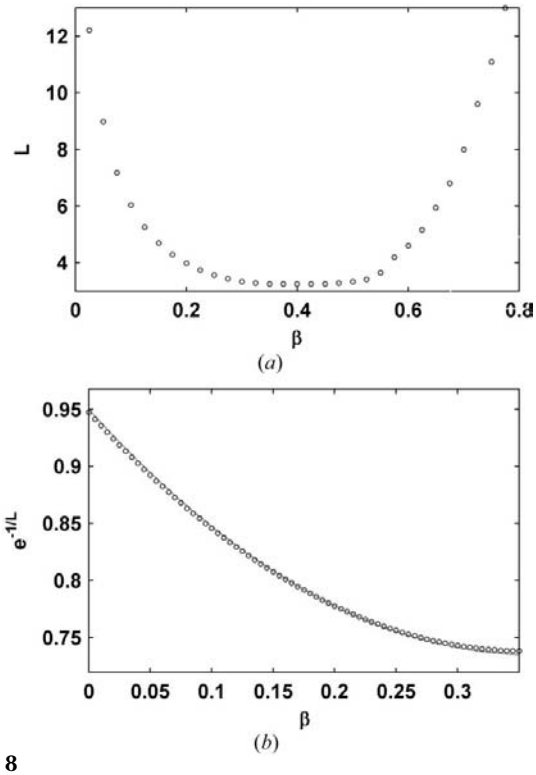

Figure 8
Variation of (*a*) the characteristic length scale (L) and (*b*) $\exp(-1/L)$ with the deformation fault probability β. Analytical results are denoted by empty circles while simulation results are denoted by the continuous curve. These results are for mixed faulting with a fixed growth fault probability $\alpha = 0.1$ and variable deformation fault probability β.

$$\tfrac{1}{2}\left\{\left[1+\frac{1-\alpha}{x}\right]\left(\frac{\alpha+x}{2}\right)^{m}+\left[1-\frac{1-\alpha}{x}\right]\left(\frac{\alpha-x}{2}\right)^{m}\right\} = \exp(-m/L). \quad (16)$$

Equation (16) describes an exact relationship between the fault probabilities and the characteristic length scale. This equation is analytically intractable in its most general form. We consider special cases for its solution.

4.1. Random deformation faults

For pure deformation faulting, an exact relationship between L and β exists, as given below on the basis of equation (16) by putting $\alpha = 0$:

$$\exp(-2/L) = 3\beta^2 - 3\beta + 1. \quad (17)$$

The functional dependence of L on β given by equation (17) is in excellent agreement with that obtained by simulation. This can be seen from Fig. 3(b) where the function $\exp(-1/L)$ is plotted against the variable β using equation (17).

4.2. Random growth faults

In the case of pure growth faulting with α in the range $0 < \alpha < 1$, we consider the two cases for $0 < \alpha < 0.536$ and $0.536 < \alpha < 1$ separately, as explained earlier. For the range $0 < \alpha < 0.536$, equation (16) is analytically intractable, but it can be solved numerically.

The variation of $\exp(-1/L)$ with α so obtained from numerical solution of equation (16) is in good agreement with that obtained by simulation as can be seen from Fig. 5(b). The small departure between the two sets of values for $\alpha > 0.3$ is due to the rounding-off of L to the nearest integer. This introduces rounding-off errors, which are especially significant for small L. Numerically, L can take any value, integer or non-integer, but only the integer values of L are physically relevant.

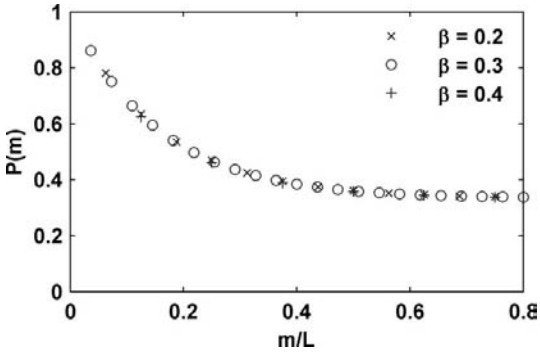

Figure 9
Variation of decay part of $P(m)$ with scaled variable m/L for different deformation fault probabilities, denoted by different symbols, exhibiting collapse of the entire data on a single master curve. These results are for mixed faulting with a fixed growth fault probability $\alpha = 0.1$ and variable deformation fault probability β.

The case $0.536 < \alpha < 1$ corresponds to region B in Fig. 1, *i.e.* $4(1-\gamma) - 2[(3-4\gamma)(1-\gamma)]^{1/2} < \alpha < 1$. ρ_e and ρ_o are now complex quantities, which may be defined as

$$\rho_e = 1/2(-\alpha + iy) = -Z\exp(-i\theta), \quad (18)$$

$$\rho_o = -1/2(\alpha + iy) = -Z\exp(i\theta), \quad (19)$$

where

$$Z = 1/2(\alpha^2 + y^2), \quad (20)$$

$$\theta = \tan^{-1}(y/\alpha) \quad (21)$$

and

$$y = -ix = \left(\{4(1-\gamma) + 2[(3-4\gamma)(1-\gamma)]^{1/2} - \alpha\} \times \{\alpha - 4(1-\gamma) + 2[(3-4\gamma)(1-\gamma)]^{1/2}\}\right)^{1/2}. \quad (22)$$

Thus,

$$Z = 2(2\alpha - 1)(1-\gamma). \quad (23)$$

The constants c_o and c_e are now given by

$$c_e = 1/2[1 + i(1-\alpha)/y] \quad (24)$$

and

$$c_o = 1/2[1 - i(1-\alpha)/y]. \quad (25)$$

Using equations (18), (19), (24) and (25), we get

$$P(m) = 1/3 + 4/3[c_r\cos(m\theta)\cos(m\pi) + c_i\sin(m\theta)\cos(m\pi)](Z)^m. \quad (26)$$

On comparing equation (26) with equation (11), we get

$$\exp(-1/L) = (2\alpha - 1)[1 - 3\beta(1-\beta)]. \quad (27)$$

Putting $\beta = 0$, we obtain for pure growth faulting

$$\exp(-1/L) = (2\alpha - 1). \quad (28)$$

It is interesting to note that equation (27) gives the exact relationship between L and α, β for region B of Fig. 1. The values for the characteristic length scale obtained by equation (28) are compared with their simulation counterparts in Fig. 6(b), which shows a reasonable agreement between the two for $0.536 < \alpha \leq 0.7$. For $\alpha > 0.7$, the simulation values are slightly less than the analytical results due to the rounding-off errors.

4.3. Mixed random growth and random deformation faults

For mixed faulting, since equation (16) is analytically intractable, we first obtain $P(m)$ *versus* m plots for different combinations of α and β numerically. We then fit equation (11) to these values to obtain the correponding L values. The values of L so obtained for $\alpha = 0.1$ and $0 < \beta < 1$ are compared with the simulation values in Fig. 8(b), which shows a good match.

5. Calculation of intensity distribution for faulted h.c.p. crystals

We have already seen that, for growth and deformation as well as for mixed faulting, $P(m)$ exhibits scaling properties. The collapse (or scaling) of $P(m)$ into master curves implies that the characteristic length scale L contains all the relevant information about the evolution of the faulted sequences. We can make use of this fact to express $I(h_3)$ solely as a function of the characteristic length scale L. Using equations (11) and (12), we performed the summation in equation (1) for an infinite size crystal ($N >> m$) and obtained the following expression for region A of Fig. 1, *i.e.* for the h.c.p.-like region:

$$I(h_3) = \frac{1-\rho^2}{N}\frac{1-\rho\cos(\pi h_3)+\rho^2}{1-2\rho^2\cos(2\pi h_3)+\rho^4}, \quad \text{where } \rho = \exp[-1/L(\xi)]. \tag{29}$$

For region B of Fig. 1, we use equations (13) and (14) and perform the summation in equation (1) to get the following expression, which has previously been derived by Shreshtha & Pandey (1996) in a different context:

$$I(h_3) = \frac{3\left[1-\rho^3\cos(3\pi h_3)\right]}{N[1-2\rho^3\cos(3\pi h_3)+\rho^6]} - \frac{\left[1-\rho\cos(\pi h_3)\right]}{N[1-2\rho\cos(\pi h_3)+\rho^2]} - \frac{1}{N}. \tag{30}$$

The intensity distributions obtained using equations (29) and (30) are shown in Fig. 10 for various cases of random deformation faulting, growth faulting and mixed faulting.

The following exact expression for the full width at half-maximum (FWHM) of the h.c.p. reflections with $h_3 = 0 \bmod 2$ and $h_3 = \pm 1 \bmod 2$ can be obtained from equation (29) for case 1 of §2 (region A of Fig. 1):

$$\mathrm{FWHM} = \frac{2}{\pi}\cos^{-1}\left\{\frac{[1-8M(1+\rho^2)+4M^2(1+\rho^2)^2]^{1/2}}{8M\rho}\right\}, \tag{31}$$

where the quantity M corresponds to the peak value of the diffracted intensity:

$$M = \frac{1-\rho+\rho^2}{1-2\rho^2+\rho^4} \quad \text{for } h_3 = 0 \bmod 2, \tag{32}$$

$$M = \frac{1+\rho+\rho^2}{1-2\rho^2+\rho^4} \quad \text{for } h_3 = \pm 1 \bmod 2. \tag{33}$$

For the f.c.c. reflections with $h_3 = \pm 2/3 \bmod 2$, the following exact expression for the FWHM can be obtained from equation (30) for case 2 of §2 (region B of Fig. 1):

$$\mathrm{FWHM} = \frac{2}{3\pi}\cos^{-1}\left(\frac{M\rho^6+M-6}{2(M-3)\rho^3}\right), \tag{34}$$

where

$$M = \frac{3(1-\rho^3)}{(1-2\rho^3+\rho^6)} \quad \text{for } h_3 = \pm 2/3 \bmod 2. \tag{35}$$

Thus the value of ρ, and hence L, may be determined from the FWHM of the broadened peaks in the observed intensity profiles. It can also be determined from the pair correlation functions obtained after the Fourier inversion of the observed

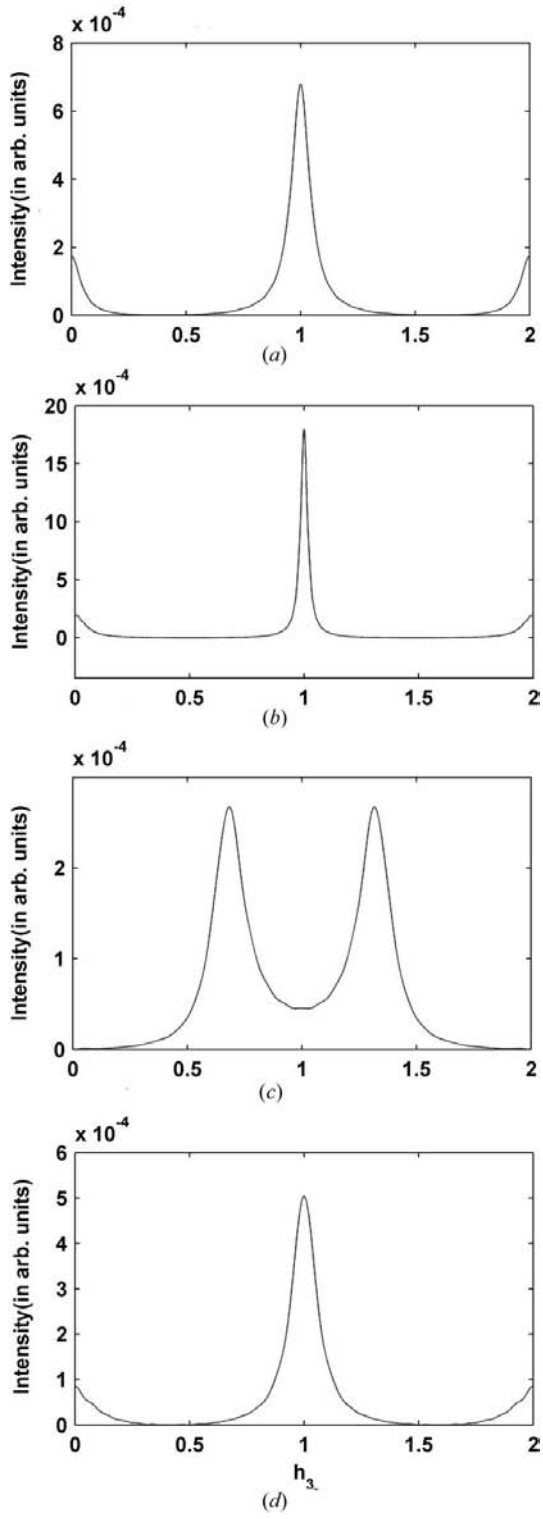

Figure 10
Diffuse intensity distributions obtained using scaling function [equations (29) and (30)] for (*a*) pure random deformation faulting with fault probability $\beta = 0.1$, (*b*) pure random growth faulting with fault probability $\alpha = 0.1$, (*c*) pure random growth faulting with fault probability $\alpha = 0.9$, and (*d*) mixed faulting with growth fault probability $\alpha = 0.1$ and deformation fault probability $\beta = 0.1$.

intensity profiles, as proposed by Shreshtha & Pandey (1996) and Estevez-Rams *et al.* (2001). From the characteristic length scale, the fault probabilities may easily be determined using the expressions given in this work.

6. Conclusions

Using the concept of characteristic length scale (L) for randomly faulted h.c.p. crystals (Shreshtha & Pandey, 1996), we have shown that the pair correlation functions for randomly faulted h.c.p. crystals exhibit scaling property, *i.e.* they can be collapsed into master curves when plotted against the interlayer separation (m) scaled with L. The relationships between the characteristic length scale and the random growth and deformation fault probabilities have been obtained. The functional dependence of L on the fault probabilities is non-universal, *i.e.* it is different for different types of stacking faults. We have also shown that the diffracted intensity distribution along $\mathbf{c}^*$ can be expressed in terms of L which can be determined from the FWHM of the experimentally observed profiles. Exact relationships between L and FWHM have also been worked out. As shown elsewhere (Tiwary & Pandey, 2007), the scaling properties of $P(m)$ are observed even for non-random faulting in h.c.p. crystals. In fact, the scaling properties of $P(m)$ hold good for all such faults in any close-packed structure such as f.c.c., 4*H*, 6*H*, 9*R etc*., provided the fault type does not retain long-range correlations.

References

Berliner, R., Fajen, O., Smith, H. G. & Hitterman, R. L. (1989). *Phys. Rev. B*, **40**, 12086–12097.

Berliner, R., Smith, H. G., Copley, J. R. D. & Triviosonno, J. (1992). *Phys. Rev. B*, **46**, 14436–14447.

Berliner, R. & Werner, S. A. (1986). *Phys. Rev. B*, **34**, 3586–3603.

Blanc, E., Burgi, H. B., Restori, R. & Schwarzenbach, D. (1996). *Europhys. Lett.* **33**, 205–210.

Estevez-Rams, E., Aragon-Fernandez, B., Fuess, H. & Penton-Madrigal, A. (2003). *Phys. Rev. B*, **68**, 064111–064122.

Estevez-Rams, E., Leoni, M., Scardi, P., Aragon-Fernandez, B. & Fuess, H. (2003). *Philos. Mag.* **83**, 4045–4057.

Estevez-Rams, E., Martinez, J., Penton-Madrigal, A. & Lora-Serrano, R. (2001). *Phys. Rev. B*, **63**, 054109–054118.

Farkas-Jahnke, M. (1973). *Acta Cryst.* B**29**, 407–413.

Hendricks, S. B. & Teller, E. (1942). *J. Chem. Phys.* **10**, 147–167.

Hirth, J. P. & Lothe, J. (1968). *Theory of Dislocations.* New York: McGraw-Hill.

Kabra, V. K. & Pandey, D. (1988). *Phys. Rev. Lett.* **61**, 1493–1496.

Kabra, V. K. & Pandey, D. (1995). *Acta Cryst.* A**51**, 329–335.

Kabra, V. K. & Pandey, D. (1996) *Phase Transit.* **59**, 199–206.

Pandey, D., Kabra, V. K. & Lele, S. (1986). *Bull. Mineral.* **109**, 49–67.

Pandey, D. & Krishna, P. (1977). *J. Phys. D*, **10**, 2957–2968.

Pandey, D. & Krishna, P. (1982). *Current Topics in Materials Science*, Vol. IX, edited by E. Kaldis, pp. 415–491. Amsterdam: North-Holland.

Pandey, D. & Krishna, P. (1992). *International Tables for Crystallography*, Vol. C, edited by A. J. C. Wilson, pp. 660–667. Dordrecht: Kluwer.

Pandey, D., Lele, S. & Krishna, P. (1980*a*). *Proc. R. Soc. London Ser. A*, **369**, 435–449.

Pandey, D., Lele, S. & Krishna, P. (1980*b*). *Proc. R. Soc. London Ser. A*, **369**, 451–461.

Pandey, D., Lele, S. & Krishna, P. (1980*c*). *Proc. R. Soc. London Ser. A*, **369**, 463–477.

Pandey, D., Prasad, L., Lele, S. & Gauthier, J. P. (1987). *J. Appl. Cryst.* **20**, 84–89.

Sato, R. (1969). *Acta Cryst.* A**25**, 387–388.

Shreshtha, S. P. & Pandey, D. (1996). *Europhys. Lett.* **34**, 269–274.

Shreshtha, S. P. & Pandey, D. (1997). *Proc. R. Soc. London Ser. A*, **453**, 1311–1330.

Shreshtha, S. P., Tripathi, V., Kabra, V. K. & Pandey, D. (1996). *Acta Mater.* **44**, 4937–4947.

Tiwary, P. & Pandey, D. (2007). In preparation.

Varn, D. P., Canright, G. S. & Crutchfield, J. P. (2002). *Phys. Rev. B*, **66**, 174110–174119.

Warren, B. E. (1969). *X-ray Diffraction.* New York: Addison Wesley.

Wilson, A. J. C. (1942). *Proc. R. Soc. London Ser. A*, **180**, 277–285.

Wilson, A. J. C. (1962). *X-ray Optics.* New York: John Wiley and Sons.

Zachariasen, W. H. (1947). *Phys. Rev.* **71**, 715–719.